THE EFFECT OF FLOW VELOCITY ON MICROCANTILEVER-BASED BIOSENSORS

M.-C. Wu [*]   **J.-S. Chang** [**]   **K.-C. Wu** [**]   **C.-H. Lin** [*]   **C.-Y. Wu** [***]

Institute of Applied Mechanics
National Taiwan University
Taipei, Taiwan 10617, R.O.C.

ABSTRACT

This work focuses on studying the effect of flow velocity on microcantilever-based biosensor by numerical simulation. The microcantilever sensors used in detecting biomolecules have attractive advantages like cost efficiency, real-time and ability of fabricating in array. Both rectangular and triangular shapes of a general model of microcantilever beam are considered. Several important physical phenomena are obtained. Comparing with the first order Langmuir theory, we have calculated the effect on the reactive rate, produced concentration, the distribution of concentration and deflection in the z axis by solving these physical coupled problem involving flow field, concentration field and chemical reaction on the reaction surface. It is found numerically that the transportation of analyte, reactive rate, the distribution of concentration and deflection in the z axis are all effected by changing the flow velocity. The result has shown that flow velocity is an important factor for this biosensor.

Keywords : Microcantilever, Biosensor, Finite element method.

1. INTRODUCTION

With the advanced in nanotechnology in recent year, biosensor is widely used to detect small biomolecules and biosensing applications have been moving toward fast. Biosensor technology is a powerful analytical technique in biological systems for its small and low-cost characteristic. Combining with chemical or physical transducer, biosensors use antibodies or other kinds of biomolecules for molecular recognition. Biomolecular recognition is a natural characteristic of the human body and many kinds of life. It has some advantages like highly sensitive, real-time, label-free and quantitative analysis on biomolecular recognition. Commonly biosensors are used as the microcantilever sensor, surface plasma resonance (SPR) and quartz crystal microbalance (QCM). These are three methods which are mostly used to detect small molecules.

Microcantilever has been proposed as mechanical transducer for recent years [1~3]. The original application comes from atomic force microscope (AFM). It is fabricated of silicon nitride and coated a gold layer to link up the specific self-assembly molecules [4~5]. The variation of the surface stress due to the combination of analytes and ligands results in the deflection of the cantilever beam [6]. Therefore, the biomolecular recognition can be translated into nanomechanical motion by using physical transducer, and then the quantitative detection of biomolecule in the solid and liquid interfaces could be obtained. Microcantilever sensors offer a platform for the label-free analysis of protein-protein interaction, enzyme reaction, and DNA hybridization [7~8].

These biosensors are usually put in the flow field to detect biomolecule and can satisfy miniaturization. The adsorption of analyte depends on two processes: mass transportation process and chemical reaction process. Langmuir *et al*. [9] brought up the first order Langmuir theory presenting the reaction model for antibody and antigen in the solid and liquid interfaces; Illkonic *et al*. [10] developed the pure diffusion-controlled model; Rahn *et al*. [11] proposed the diffusion limited Langmuir model; Nicholas *et al*. [12] had proved that under low concentration and low flow velocity, the thickness of diffusion layer will have effect on reaction rate. Therefore flow velocity will be an important factor for the development of thickness of diffusion layer.

In this work, we present a model for the microcantilever sensor relationship to establish the effect by flow velocity and to derive the relation of reactive rate, produced concentration, the distribution of concentration and deflection in the *z* axis. The finite element numerical simulation was built and set up on COMSOL Muityphysics. Comparing with different flow velocities, the results have shown that faster flow velocity will get more remarkable effects.
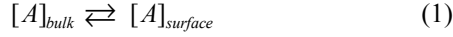
---

[*] Graduate student   [**] Professor   [***] Ph.D. student
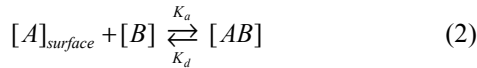
2. MATHEMATICAL MODEL

In the solid-liquid interface, the reaction has two step events:

Mass transportation process: The analyte is transferred out of the bulk solution towards the reaction surface.

$$[A]_{bulk} \rightleftarrows [A]_{surface} \qquad (1)$$

Chemical reaction process: The binding of the analyte to the ligand take place.

$$[A]_{surface} + [B] \underset{K_d}{\overset{K_a}{\rightleftarrows}} [AB] \qquad (2)$$

where $[A]_{bulk}$ is the analyte in the bulk, $[A]_{surface}$ is the analyte on the gold surface with ligand bound to the dextran matrix, $[B]$ is the ligand , $[AB]$ is the analyte-ligand complex, K_a is the association rate constant, and K_d is the dissociation rate constant.

2.1 Governing Equations of the Flow Field

We assume that the density ρ and viscosity η of the modeled fluid are constant, that is, they are not affected by temperature and concentration. The governing equations of continuity and three-dimensional momentum can be expressed as follows:

$$\nabla \cdot \vec{V} = 0 \qquad (3)$$

$$\rho \frac{\partial u}{\partial t} + \rho \vec{V} \cdot \nabla u - \eta \nabla^2 u + \frac{\partial p}{\partial x} = 0 \qquad (4)$$

$$\rho \frac{\partial v}{\partial t} + \rho \vec{V} \cdot \nabla v - \eta \nabla^2 v + \frac{\partial p}{\partial y} = 0 \qquad (5)$$

$$\rho \frac{\partial w}{\partial t} + \rho \vec{V} \cdot \nabla w - \eta \nabla^2 w + \frac{\partial p}{\partial z} = 0 \qquad (6)$$

where u, v, w are the velocity components in the x, y, z directions, respectively; η is dynamic viscosity of the fluid; ρ is density of the fluid; p is the pressure.

No-slip boundary conditions are assumed between the inter faces of the microcantilever and the flow. A total load $\vec{F}$ from the flow, consisting of a pressure component and a viscous drag component, is applied to the boundary of this structure. This load, defined as force per area, equals:

$$\vec{F} = \vec{n} \cdot (-pI + \eta(\nabla \vec{u} + (\nabla \vec{u})^T)) \qquad (7)$$

where p is the fluid pressure; I is the unit tensor; η is the dynamic viscosity; $\vec{u}$ is the velocity field; $\vec{n}$ is the normal unit vector of the boundary pointing out from the fluid. If this load is not small, negligible disturbance will be produced during the measurement of deflection of the microcantilever due to surface stress.

2.2 Governing Equations of Concentration Field

Transportation of the protein from the flow to the surface is caused by fluid flow and diffusion. In order to solve the problem, we apply Fick's Second Law.

$$\frac{\partial [A]}{\partial t} + u\frac{\partial [A]}{\partial x} + v\frac{\partial [A]}{\partial y} + w\frac{\partial [A]}{\partial z}$$
$$= D\left(\frac{\partial^2 [A]}{\partial x^2} + \frac{\partial^2 [A]}{\partial y^2} + \frac{\partial^2 [A]}{\partial z^2} \right) \qquad (8)$$

where $[A]$ is the concentration of analyte; and D is the diffusion coefficient.

2.3 Governing Equations of Reaction Surface

The reaction between an immobilized ligand and analyte can be assumed to follow the first order Langmuir adsorption model. During the association phase, the complex $[AB]$ increases as a function of time according to：

$$\frac{\partial [AB]}{\partial t} = K_a[A]_{surface}\{[B]-[AB]\} - K_d[AB] \qquad (9)$$

The relation between concentration gradients on the surface and the rate of reaction is given by

$$-D\frac{\partial [A]_{surface}}{\partial y} = K_a[A]_{surface}\{[B]-[AB]\} - K_d[AB] \qquad (10)$$

where $[A]_{surface}$ is the analyte at the gold surface with ligand bounded to the dextran matrix; $[B]$ is the ligand, $[AB]$ is the analyte-ligand complex; K_a is the association rate constant; and K_d is the dissociation rate constant.

3. SIMULATION AND RESULTS

Simulation and modeling for microcantilever sensor are conducted using COMSOL Muityphysics. The microcantilever is fabricated by silicon nitride and takes the size as 230μm in length, 40μm in width and 3μm in thickness for rectangular microcantilever, take the size as 200μm in height, 40μm in each leg and form with 45 degree for triangular microcantilever. The size of flow chamber is 500μm in width and length, 100μm in height. The material parameters are listed on the Table. 1.

3.1 The Difference Between the First Order Langmuir Theory and Simulation

This simulation takes more time to allow the results to reach the steady state than the first order Langmuir adsorption theory does. $[A]_{surface}$ is not equal to $[A]_{bulk}$ until the reaction is over. The absorption limitation in this simulation means that the diffusion is too slow for the analyte to reach the reactive surface and can not chemically reacted with the ligand when the flow velocity is too slow, the diffusion coefficient is small and k_a is

Table 1 Parameters of FEM simulation

Property	Value
Young's Modulus of SiN	150 GPa
Poisson ratio of SiN υ	0.23
Density of SiN	2330kg/m^3
Mass damping parameter	1 1/s
Stiffness damping parameter	0.001s
Flow density ρ	1×10^3kg/m^3
Diffusion coefficient	1×10^{-10}m^2/s
Association rate constant K_a	2000M^{-1}S^{-1}
Dissociation rate constant K_d	0.001S^{-1}
Concentration of $[A]_{bulk}$	1×10^{-5}M
Concentration of $[B]$	1×10^{-8}mole/m^2
Dynamic viscosity η	1×10^{-3} Pa·S

high. From Fig.1 we know that $[A]_{surface}$ will reach $[A]_{bulk}$ soon when the flow velocity is 1e-1 (m/s) unless the speed of rate of absorption is greater than the speed of rate of $[A]_{bulk}$ initially. The concentration is closer to the first order Langmuir theory as the flow velocity is faster. As the ligand combines with analyte, the trends of this simulation shown in Fig. 2 is approximately the same as that shown in Fig. 1. It takes more time to reach the steady state than the first order Langmuir adsorption theory does.

3.2 The Effect of Different Flow Velocity on Reactive Rate and Time for Steady State

We compare the reactive rates for the two different shapes of microcantilevers with different inlet velocities (1e-4, 1e-3, 1e-2, 1e-1m/s). The result for steady state is listed on the Table 2. From the table we know that the faster the flow velocity, the faster the concentration to reach the steady state. From the reactive rates we know that the slower the flow velocity, the longer the time to reach the fastest reactive rate by mass transport process, and the fastest reactive rate for low velocity is much lower than that for the high flow velocity as Figs. 3 and 4. Since the produced concentration on left side of the triangular microcantilever is higher than that on the right side and the concentration is not uniform, the reactive rate is slower than the rectangular one as Fig. 5.

3.3 The Effect of Different Flow Velocity for Produced Concentration Distribution

From Figs. 6 and 7 it can be seen that the slower the flow, the thicker the thickness of the diffusion layer. The trend is described as the equation $\delta = D^{\frac{1}{3}} v^{\frac{1}{6}} \sqrt{\frac{x}{u}}$ which is derived from Jung *et al* [13], where δ is the thickness of the diffusion layer; D is the diffusion coefficient; v is Kinematic viscosity; u is the flow velocity in x direction; x is the position from the reactive surface where we get the data point. Figure. 8 shows the concentration distribution profile of [A] for rectangular microcantilever. The produced concentration distribution
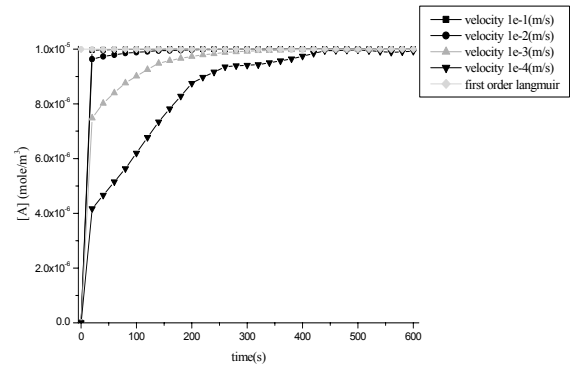
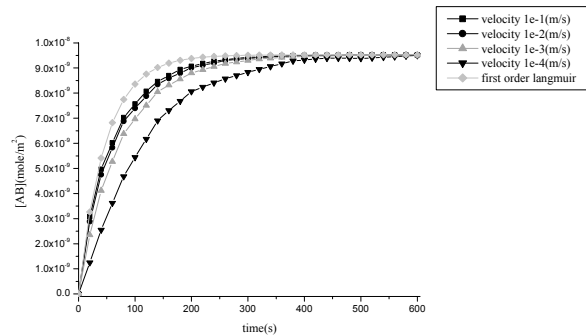Fig. 1 $[A]_{surface}$ *vs*. time in different flow velocity with the first Langmuir theory

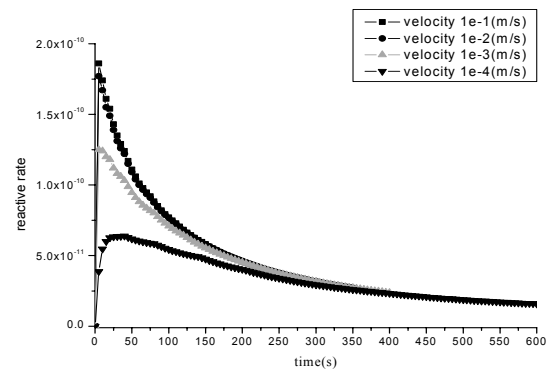Fig. 2 $[AB]$ *vs*. time in different flow velocity with Langmuir Theory

Fig. 3 Reactive rate *vs*. time for rectangular microcantilever
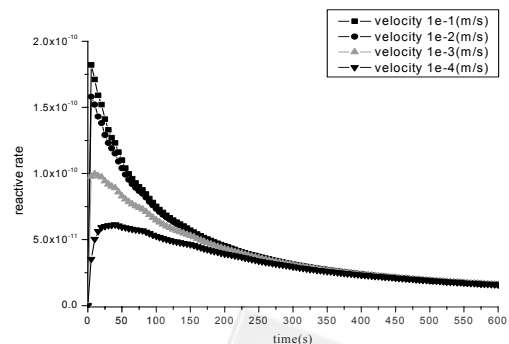

Fig. 4 Reactive rate *vs*. time for triangular microcantilever

Table 2   Time reguired to reach steady state for different shapes of microcantilevers under various flow velocities

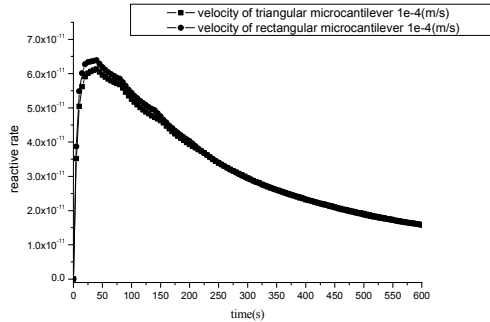| Velocity (m/s)	1e-1	1e-2	1e-3	1e-4
rectangular (s)	320	320	345	590
triangle (s)	380	380	405	640

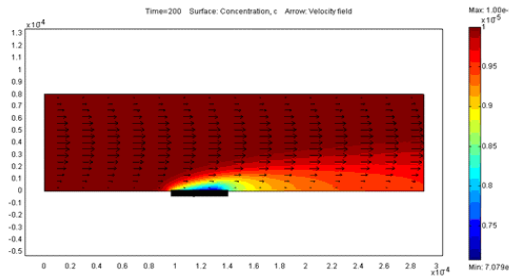Fig. 5   Reactive rates for triangular and rectangular microcantilever at flow speed 1×10^{-4} (m/s)

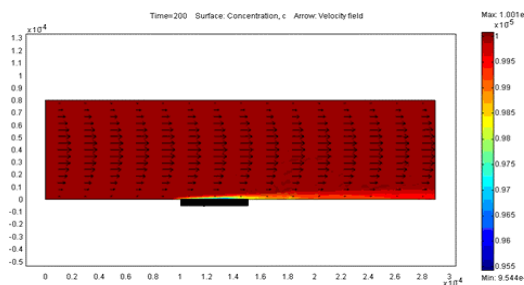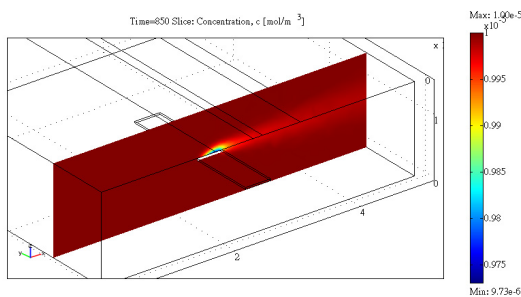Fig. 6   The distribution of concentration for flow velocity 1×10^{-4} (m/s)

Fig. 7   The distribution of concentration for flow velocity 1×10^{-2} (m/s)

Fig. 8   The concentration distribution on rectangular microcantilever for flow velocity 1×10^{-4} (m/s)

of [AB] on the surface is plotted on the Figs. 9 and 10. We use the cutting line to observe the concentration distribution on the surface as Fig. 11. The concentration which is near the inlet is a little higher. The coverage rate will differ by 20% at the same time (60sec) with flow velocity 1e-4 (m/s) on the surface of microcantilever with width of 40μm as plotted on Figs. 12 and 13. Because the two sides of the reactive surface are closer to the fluid, the concentrations at the edges comparing to that at the central place will be higher. Figures 14 and 15 reveal coverage with varying time.
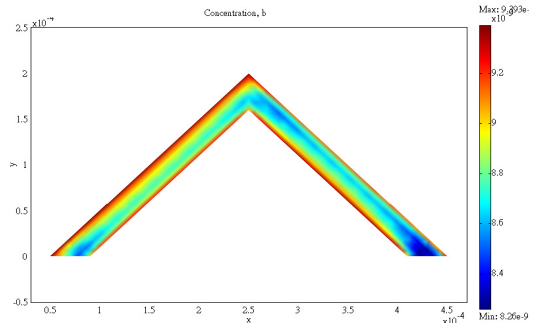

Fig. 9   The produced concentration distribution of [AB] for triangular microcantilever
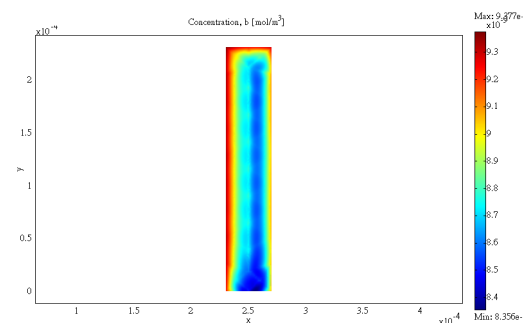

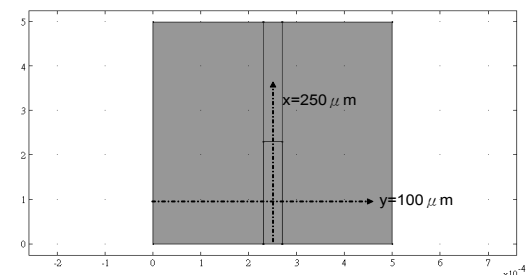Fig. 10   The produced concentration distribution of [AB] for triangular microcantilever

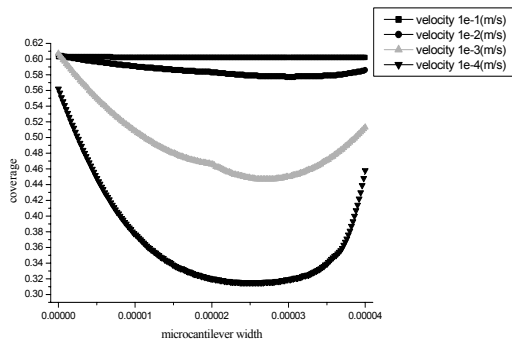Fig. 11   The two cutting line for microcantilever ($x = 250 \times 10^{-6}$m $y = 100 \times 10^{-6}$m)

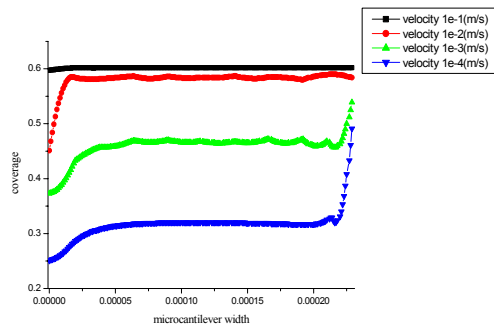Fig. 12 (y = 100 × 10⁻⁶m) rectangular microcantilever width coverage *vs*. after 60 seconds of operation

Fig. 13 (x = 250 × 10⁻⁶m) rectangular microcantilever width coverage *vs*. after 60 seconds of operation

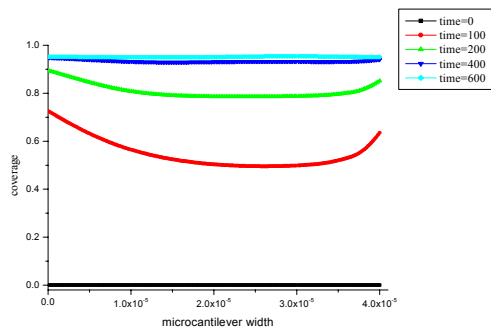Fig. 14 (y = 100 × 10⁻⁶m) rectangular microcantilever width coverage *vs*. with time varying changing with flow velocity 1e-4
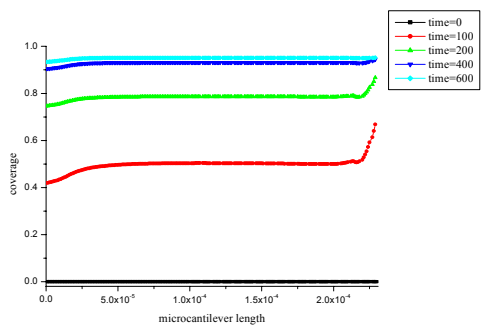

Fig. 15 (x = 250 × 10⁻⁶m) rectangular microcantilever width coverage *vs*. with time varying changing with flow velocity 1×10^{-4}

3.4 Deflection Analysis for Microcantilever in Different Flow Velocity

We simulate triangular and rectangular microcantilevers at different place in three dimension flow tunnel as Figs. 16 and 17 and compare different inlet flow velocity 1e-4, 1e-3, 1e-2, 1e-1 (m/s) which has effect on deflection by shear force and pressure distribution. The force can be described as the Eq. (2)~(7). The deflections of these two kinds of microcantilever at three positions (75μm, 50μm, 25μm from the bottom) are listed in Tables 3 and 4. Theoretically the deflection of microcantilever placed in different places should be the same, but actually it will be a little different by mesh grid which we use. The microcantilever should be put in its central place (in the z-direction) to avoid the disturbance of deflection from the flow field. It may produce an 8 ~ 10 (nm) deflection at flow velocity 1e-1 (m/s) when the microcantilever is put at the position 75(μm) or 25(μm) in the *z*-direction.
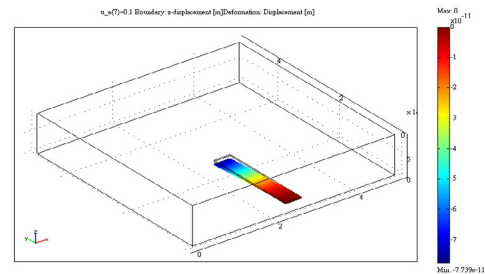

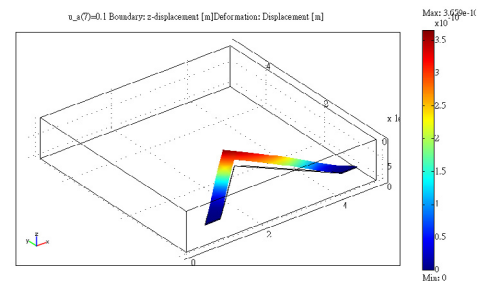Fig. 16 The deformation of rectangular microcantilever

Fig. 17 The deformation of triangular microcantilever

Table 3 Deflection of the triangle microcantilever due to velocity effects

Velocity (m/s)	1e-1	5e-2	1e-2	5e-3	1e-3	5e-4	1e-4
deflection (nm) at 75μm height	−1.01E1	−2.45	−6.25E-2	−4.54E-3	3.38E-3	1.96 E-3	4.34E-4
deflection (nm) at 50μm height	2.32E-2	4.35E-3	1.20E-3	6.59E-4	1.43E-4	7.22E-5	1.46E-5
deflection (nm) at 25μm height	1.02 E1	2.50	6.66 E-2	6.24E-3	−3.09E-3	−1.82E-3	−4.07E-4

Table 4 Deflection of the rectangle microcantilever due to velocity effects

Velocity (m/s)	1e-1	5e-2	1e-2	5e-3	1e-3	5e-4	1e-4
deflection (nm) at 75μm height	−7.96	−2.13	−8.62E-2	−2.15E-2	−8.32E-4	−1.99E-4	−5.22E-5
deflection (nm) at 50μm height	−9.87E-3	−2.98E-3	−5.86E-4	−3.02E-4	−6.23E-5	−3.13E-5	−6.27E-6
deflection (nm) at 25μm height	7.95	2.14	8.55E-2	2.10E-2	7.12E-4	1.38E-4	−7.20E-6

4. CONCLUSIONS

A simple microcantilever model has been set up to simulate physical phenomenon in three dimensional flow field.　We get some important conclusions:

1. The concentration of [AB] complex will be close to that given by the first order Langmuir theory when the flow velocity is high.

2. The faster the flow velocity, the faster the reactive rate to reach the steady state.

3. Compared the inner part of the reactive surface, the leading and the trail sides have high concentrations of [AB] complex.

4. The faster the flow velocity will induce a larger deflection in the z-axis, and the microcantilever should be put in a central place to avoid the disturbance of deflection from the flow field.

ACKNOWLEDGEMENTS

REFERENCES

1. Battiston, F. M., Ramseyer, J. P., Lang, H. P., Baller, M. K., Gerber, Ch., Gimzewski, J. K., Meyer, E. and Guntherodt, H. J., "A Chemical Sensor Based on a Microfabricated Cantilever Array With Simultaneous Resonance-Frequency and Bending Readout," *Sensor and Actuators B*, 77, pp. 122−131 (2001).

2. Yoo, K. A., Na, K. H., Joung, S. R., Nahm, B. H., Kang, C. J. and Kim, Y. S., "Microcantilever-Based Biosensor for Detection of Various Biomolecules," *Japanese Journal of Applied Physics*, 45, 1B, pp. 515−518 (2006).

3. Moulin, A. M., O'Shea, S. J. and Welland, M. E., "Microcantilever-Based Biosensors," *Ultramicroscopy*, 82, pp. 23−31 (2000).

4. Berger, R., Delamarche, E., Lang, H. P., Gerber, C., Gimzewski, J. K., Meyer, E. and Güntherodt, H. J., "Surface Stress in the Self-Assembly of Alkanethiols on Glod," *SCIENCE*, 276, pp. 2021−2024 (1997).

5. Poirier, G. E. and Pylant, E. D., "The Self-Assembly Mechanism of Alkanethiols on Au(111)," *Science, New Series*, 272(5265), pp. 1145−1148 (1996).

6. Raiteri, R., Butt, H. J. and Grattarola, M., "Changes in Surface Stress at Liquid/Solid Interface Measured with a Microcantilever," *Electrochimica Acta*, 46, pp. 157−163 (2000).

7. Wu, G., Datar, R. H., Hansen, K. M., Thundat, T., Cote, R. J. and Majumdar, A., "Bioassay of Prostate-Specific Antigen (PSA) Using Microcantilevers," *Nature Biotechnology*, 19, pp. 856−860 (2001).

8. Wu, G., Ji, H., Hansen, K., Thundat, T., Datar, R., Cote, R., Hagan, M. F., Chakraborty, A. K. and Majumdar, A., "Origin of Nanomechanical Cantilever Motion Generated from Biomolecular Interactions," *Proceedings of the National Academy of Sciences of the United States of America* 98, pp. 1560−1564 (2001).

9. Langmuir, I., "The Adsorption of Gases on Plane Surfaces of Glass, Mica and Platinum," *J. Am. Chem. Soc.,* 40, pp. 1361−1403 (1918).

10. Ilkovic, D., *Collect. Czech. Chem. Commun.,* 6, p. 498 (1934)

11. Rahn, J. R. and Hallock, R. B., "Antibody Binding to Antigen-Coated Substrates Studied with Surface Plasmon Oscillations," *Langmuir*, 11, pp. 650−654 (1995).

12. Nicholas Camillone, "Diffusion-Limited Thiol Adsorption on the Gold(111) Surface," *Langmuir*, 20, pp. 1199−1206 (2004).

13. Jung, L. S. and Campbell, C. T., "Sticking Probabilities in Adsorption of Alkylthiols from Liquid Ethanol Solution onto Gold," *J. Phys. Chem. B,* 104, pp. 11168−1117 (2000).